Asian Journal of Pharmaceutical Sciences 18 (2023) 100782

Available online at www.sciencedirect.com

ScienceDirect

journal homepage: www.elsevier.com/locate/AJPS

Original Research Paper

Water-responsive gel extends drug retention and facilitates skin penetration for curcumin topical delivery against psoriasis

Qing Yao[a,b,1], Yuan-Yuan Zhai[a,b,1], Zhimin He[b,1], Qian Wang[b], Lining Sun[a,c], Tuyue Sun[a], Leyao Lv[a], Yingtao Li[a], Jiyong Yang[e], Donghui Lv[e], Ruijie Chen[a,c], Hailin Zhang[a,*], Xiang Luo[f,*], Longfa Kou[a,c,d,*]

[a] Wenzhou Municipal Key Laboratory of Pediatric Pharmacy, Department of Pharmacy, The Second Affiliated Hospital and Yuying Children's Hospital of Wenzhou Medical University, Wenzhou 325027, China
[b] School of Pharmaceutical Sciences, Wenzhou Medical University, Wenzhou 325035, China
[c] Key Laboratory of Structural Malformations in Children of Zhejiang Province, Wenzhou 325027, China
[d] Wenzhou key Laboratory of basic science and translational research of radiation oncology, Wenzhou 325027, China
[e] Beijing Baoyi Technology Co., Ltd, Beijing 101115, China
[f] Institute of Pharmaceutics, Shaoxing University, Shaoxing 312000, China

ARTICLE INFO

Article history:
Received 27 September 2022
Revised 5 January 2023
Accepted 18 January 2023
Available online 1 February 2023

Keywords:
Psoriasis
Sol-gel transition
Water-responsive
Curcumin
Topical drug delivery

ABSTRACT

Psoriasis is a chronic inflammatory skin disease characterized by erythema, scaling, and skin thickening. Topical drug application is recommended as the first-line treatment. Many formulation strategies have been developed and explored for enhanced topical psoriasis treatment. However, these preparations usually have low viscosity and limited retention on the skin surface, resulting in low drug delivery efficiency and poor patient satisfaction. In this study, we developed the first water-responsive gel (WRG), which has a distinct water-triggered liquid-to-gel phase transition property. Specifically, WRG was kept in a solution state in the absence of water, and the addition of water induced an immediate phase transition and resulted in a high viscosity gel. Curcumin was used as a model drug to investigate the potential of WRG in topical drug delivery against psoriasis. *In vitro* and *in vivo* data showed that WRG formulation could not only extend skin retention but also facilitate the drug permeating across the skin. In a mouse model of psoriasis, curcumin loaded WRG (CUR-WRG) effectively ameliorated the symptoms of psoriasis and exerted a potent anti-psoriasis effect by extending drug retention and facilitating drug penetration. Further mechanism study demonstrated that the anti-hyperplasia, anti-inflammation, anti-angiogenesis, anti-oxidation, and immunomodulation properties of curcumin were amplified by enhanced topical drug delivery efficiency. Notably, neglectable

* Corresponding authors.
E-mail addresses: zhlwz97@hotmail.com (H. Zhang), xiangluo@usx.edu.cn (X. Luo), klfpharm@163.com (L. Kou).
[1] These authors contributed equally to this work.
Peer review under responsibility of Shenyang Pharmaceutical University.

https://doi.org/10.1016/j.ajps.2023.100782

local or systemic toxicity was observed for CUR-WRG application. This study suggests that WRG is a promising formulation for topically psoriasis treatment.

1. Introduction

Psoriasis is an autoimmune skin disease affecting 2%–3% of people worldwide, characterized by erythema, scaling, and skin thickening [1–3]. These pathological skin conditions mainly result from keratinocyte proliferation, epidermal hyperplasia, increased angiogenesis, and extensive infiltration of immune cells. According to the disease progression, current psoriasis treatments include topical application of retinoic acid-based regimens (acitretin, methotrexate), corticosteroids (dexamethasone, betamethasone [4]), and vitamin D3 (calcipotriol) [5], phototherapy [6] (photodynamic [7], photochemotherapy [8]), and other biological agents [9,10]. But, these strategies are all still far from satisfactory. For example, topical application of corticosteroids usually causes skin irritation, and the treatment is often compromised due to low drug retention and penetration [11]. As for phototherapy, the anti-psoriasis therapeutic outcome is always delayed, and the risk of skin cancer also restrains its application. Biological agents, like antibodies against tumor necrosis factor-α (TNF-α) and interleukin-17 (IL-17), have shown impressive therapeutic efficacy in severe psoriasis patients by suppressing TNF-α/IL-17-involved inflammation. But it is important to note that long-term immunosuppression could boost the risk for affection and cancer initiation. As such, further investigations are urgently required to develop alternative therapeutic options.

Topical application is still an attractive alternative for psoriasis treatment due to the non-invasive delivery manner, limited side effects, and improved patient compliance. The major challenge for topical drug delivery is the skin's barrier function. Healthy skin contains an intact stratum corneum, which largely reduces the penetration of drug molecules. However, in psoriasis skin, increased proliferation and decreased differentiation of keratocytes, as well as the inflammation-associated increased vascular permeability and vasodilatation, contribute to the partial loss of barrier function of the skin, providing a preferable area for topical application of drugs for psoriasis treatment. Many newly reported novel drug delivery systems, like nanoparticles, liposomes, micelles, solid lipid nanoparticles, and dendrimers, have been explored for topically drug delivery. Nevertheless, these novel preparations usually have low liquid viscosity, and their retention on skin surface was insufficient, leading to an unsatisfactory drug delivery efficiency and reduced therapeutic outcome [12,13]. Though the thickening regents have been used to increase the viscosity of these new preparations, the nanostructure stability, drug solubility, and drug penetration could also be affected, which might compromise the delivery efficiency. For example, carboxymethylcellulose increased the emulsion but decreased the skin penetration of capsaicin [14]. Therefore, the formulation that has high viscosity to extent drug retention on the skin surface and keeps enhanced drug penetration performance is strongly required for psoriasis therapy.

In this study, we developed a water-responsive gel (WRG) that holds a solution state in the absence of water but converted to a gel state with a considerable viscosity in the presence of water. This is the first gel formulation with water-triggered liquid-to-gel phase transition property for psoriasis use to our best knowledge. Our data indicated that WRG exhibited high viscosity after gelation and increased skin retention and drug permeation into the skin tissue. These features are quite suitable for topical drug delivery for psoriasis treatment. Hydrogels have already been used for psoriasis treatment for many years. Compared to traditional hydrogel, WRG prepared here displayed additional advantages, including enabling hydrophobic drug fully dissolved, easier smearing, keeping skin surface moistened within a longer time, etc., beneficial for topical drug delivery for prsoriasis treatment. Curcumin, a natural polyphenolic ingredient of the spice turmeric possessing strong anti-oxidative and anti-inflammatory properties [15–20], was used as a model drug. The water-responsive gelation and physicochemical properties of the WRG were investigated. We systemically studied the anti-psoriasis efficacy of CUR-WRG in the imiquimod (IMQ)-induced psoriasis mouse model. CUR-WRG could significantly improve the drug delivery efficiency and attenuate the psoriasis symptoms by reducing inflammation, oxidative stress, and angiogenesis and inhibiting T lymph cells recruitment (Scheme 1).

2. Materials and methods

2.1. *Materials*

Curcumin (CUR) was purchase from Macklin (Shanghai, China). Phosphatidylcholine (PC) was purchased from Lipoid (Ludwigshafen, Germany). Glyceryl Dioleate (GDO) was bought from Shanghai Wencai New Materials Technology Co., Ltd. (Shanghai, China). Propylene glycol (PG), Tween 80, Dialysis bag (molecular weight cut-off: 7000 Da), Hematoxylin and Eosin (H&E) staining kit, Malondialdehyde (MDA) and Superoxide dismutase (SOD) kit were purchased from Solarbio (Beijing, China). IL-17 and IL-22 enzyme-linked immunosorbent assay (ELISA) kits were obtained from Jianglai Biological (Shanghai, China). Indocyanine green (ICG) (MB4675) was bought from Meilun Biotechnology Co., Ltd. (Dalian, China). The anti-Ki67 (ab 15580), anti-VEFG (ab1316) and anti-MPO (ab65871), and donkey anti-rabbit IgG H&L

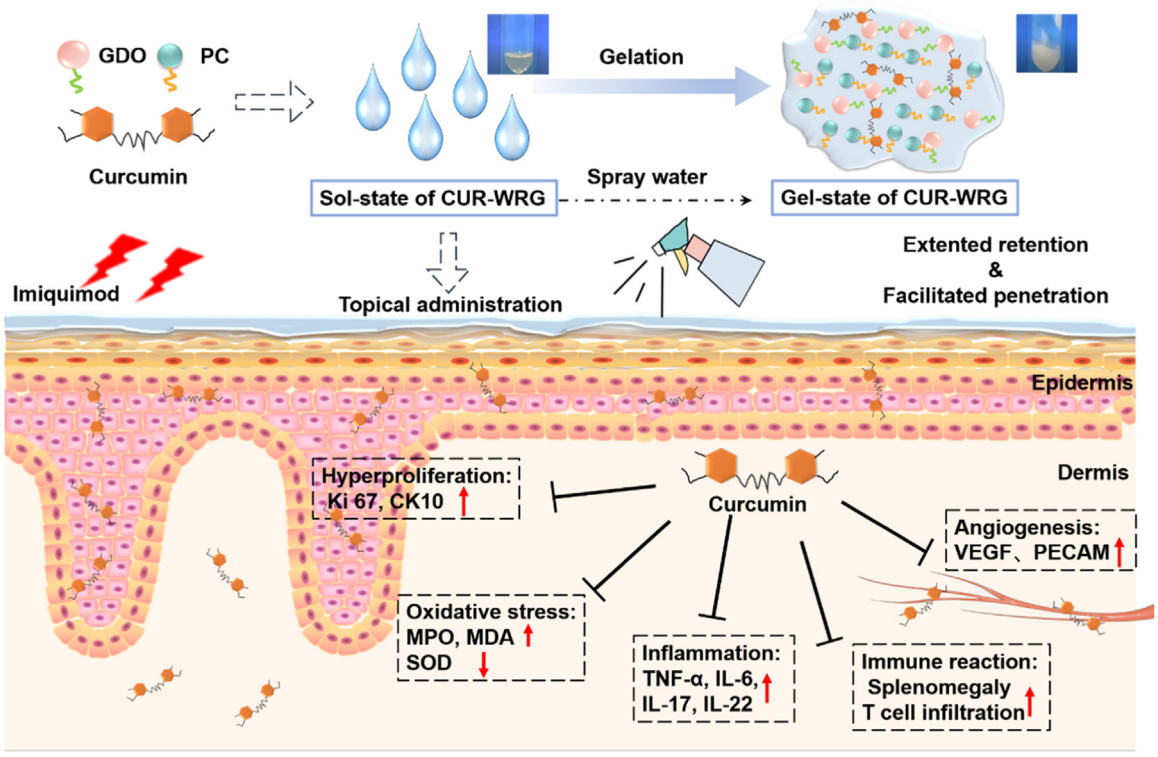

Scheme 1 – Curcumin loaded water-responsive gel (CUR-WRG) ameliorates psoriasis-like inflammation by inhibiting hyperproliferation, inflammation, and angiogenesis.

(Alexa Fluor® 647) were obtained from Abcam (MA, US). The anti-CD4 (bs-0647R) and anti-CD8 (bs-0648R) were purchased from BIOSS company (Beijing, China). The anti-cytokeratin 10 (CK 10, AF0197), anti-IL-6 (DF6087) were bought from Affinity Biosciences (OH, USA). The anti-PECAM (sc365804) was provided by Santa Cruz Biotechnology (TX, USA). 5% Imiquimod (IMQ) cream was purchased from Sichuan Ming Xin Pharmaceutical Co., Ltd. (Chengdu, China). Acetonitrile, ethanol, and methanol were all of HPLC grade.

2.2. *Animals and cell lines*

Healthy male BALB/c mice (4–6 weeks, 20–22 g) were purchased from Shanghai Laboratory Animal Center (Shanghai, China) and bred in a specific-pathogen-free environment in the animal center of Wenzhou Medical University. All animal studies were performed in accordance with the Guidelines for Animal Experimentation of Wenzhou Medical University, and the protocols were approved by the Animal Ethics Committee of Wenzhou Medical University.

The human immortalized keratinocytes (HaCaT) cells were purchased from Hunan Fenghui Biotechnology Co., Ltd. (Changsha, China). HaCaT were grown in a high glucose-DMEM medium with 10% (v/v) FBS under a humidified 5% CO_2 incubator at 37 °C.

2.3. *Preparation and characterization of WRG*

Ethanol (5.5%, w/w), PG (10%, w/w), and Tween 80 (4.5%, w/w) were firstly mixed in a 2 ml tube, and then PC (35%, w/w) and GDO (45%, w/w) were added and fully dissolved. The formed solution was vortexed and probe-sonicated for homogenization and then stored at 4 °C. This obtained solution was named WRG, which presented as a solution state (Sol). For gelation, double stilled water was added into the WRG Sol with different weight ratios (1:10, 2:10, 3:10, and 4:10). For curcumin loaded water-responsive gel (CUR-WRG) preparation, CUR was firstly dissolved in the mixture of Ethanol, PG and Tween 80, and the following steps were same as described above. To track the drug in WRG, ICG was selected as a fluorescence probe. For ICG-WRG, ICG was firstly dissolved in the mixture of Ethanol, PG, and Tween 80, and the following steps were the same as described above.

The water triggered sol-gel transition process in the tube was first observed by the naked eye [21], and the recrystallization during the sol-gel transition process was visualized and recorded under the polarized light microscope (PLM, Axio Scope.A1, ZEISS, Germany) at 25 ± 0.5 °C. To explore the water responsive property and adhesion ability of WRG, the WRG sol was smeared onto a tin sheet, and then the coated sheet was immediately immersed into the double-distilled water and directly contacted to the tube wall. Water could initiate the gelation, and the sheet contacting to tube wall could indicate the adhesion ability of WRG. The binding sheet was photographed at designed time intervals. In addition, the viscosity, viscoelasticity, and thixotropy were measured using the rheometer (the TRILOS RH-x) with a cone plate (diameter of 30 mm). The gap distance was set at 1 mm. The viscosities and shear-thinning behaviors of the WRG were tested with shear rates ranging from 0 to 100 rad/s.

2.4. *In vitro drug release*

The *in vitro* release behavior of CUR from WRG was evaluated using a modified dialysis method [22,23]. Briefly, 1 mL of CUR-WRG was added into the dialysis bag (molecular weight cut-off: 7000 Da), which was then sealed from the two ends and immersed into 10 ml pH 7.4 PBS medium containing 0.5% sodium dodecyl sulfonate under a horizontal shaker (25 °C, 200 rpm). At predetermined time intervals (0, 1, 2, 4, 8, 12, 24 and 48 h), 1 ml the sample was collected, and the same fresh medium was replenished. The collected samples were diluted with acetonitrile, filtered (0.22 μm) and then analyzed using a modified HPLC method [24]. Briefly, the mobile phase was the mixture of acetonitrile and 0.4% (v/v) acetic acid solution in the ratio of 65:35; isocratic elution was applied, and the flow rate was 1.0 ml/min; the wavelength for detection was set at 428 nm. A thermo-scientific reverse-phase C_{18} column (5 μm, 4.6 mm × 250 mm) was applied for all analyses, and the column temperature was kept at 30 °C.

2.5. *MTT assay*

The safety of WRG or CUR-WRG was evaluated using an MTT assay. Briefly, HaCaT cells were seeded in a 96-well plate with the density of 5×10^3 cells/well and allowed for adherence overnight. WRG or CUR-WRG with different concentrations were used to treat cells, respectively, for 12 h. After that, the cells were incubated with 0.5 mg/mL MTT solution at 37 °C for 3 h. After removing the MTT solution, DMSO (150 μl) was added to each well and incubated for 30 min to dissolve the formazan. The absorbance at 492 nm was measured using a microplate reader (Spectra Max; Molecular Devices, Sunnyvale, CA, USA).

2.6. *In vivo biocompatibility of WRG*

The *in vivo* biocompatibility of WRG was investigated using healthy BALB/c mice. Briefly, WRG was subcutaneously injected or topically smeared on the back of mice. After 1 d or 3 d, the mice were sacrificed, and the skin tissues in the treated area and out of the area were collected for observation and histological analysis. In addition, the major organs, including the heart, liver, spleen, lung, and kidney, were also collected, fixed in 4% paraformaldehyde, embedded in paraffin, sliced, and stained with H&E. All sections were visualized and recorded using Nikon inverted microscope (Japan).

2.7. *Evaluation of drug penetration into the skin*

ICG was selected as a fluorescence probe to monitor the drug penetration into the skin. The concentration of ICG loaded into WRG was kept as 100 μg/ml, and free ICG was used as a control. The BALB/c mice were shaven on the ear side 24 h before the experiment. ICG loaded WRG (ICG-WRG) and ICG were applied topically to the shaven ear region of mice and kept under dark conditions. After 3 h, the animals were sacrificed, and their ears were excised. After washing with PBS for three times, the ears were mounted between glass slides and imaged with a Leica laser-scanning confocal microscope (TCS SP8, Oberkochen, Germany). The photographs were captured at sequential 3 μm intervals from the skin surface. The orthogonal view of the skin was reconstructed using the X-Z sectioned images to visualize the vertical trends of ICG penetration. Quantitative analysis was performed by using the microscope-matched software.

2.8. *IMQ-induced psoriasis model and topical application of CUR-WRG*

The psoriasis model was constructed using the same method we reported in our previous study [25]. Briefly, the hair on the mouse's back or ear was shaved the day before the experiment, and 5% IMQ cream was then topically applied (Day 0) on the mouse's back or ear skin for seven days unless otherwise stated. Mice were randomly divided into 4 groups (6 mice in each group). The CUR-WRG (30 μM, 200 μl) was smeared on the shaved ear or back on predesigned time points, and then water was sprayed for rapid gelation. CUR was firstly dissolved in ethanol and then diluted with double-distilled water, and the same dose of CUR was used as a control. All applications and treatments were conducted under anesthesia. The severity of skin inflammation was monitored and evaluated based on the clinical Psoriasis Area Severity Index (PASI) [26]. The body weight was also recorded every day. After the experiments, the serum, full-thickness skin samples, and the spleen of mice were all collected for further analysis.

2.9. *Histological assessment*

The collected skin tissue and spleen were fixed, embedded, and sliced into 5-μm sections. As previously reported, the tissue sections were deparaffinized and stained with H&E for analysis [27]. For immunohistochemical assay, the sections were incubated with anti-Ki 67 (1:200), anti-CK 10 (1:200), anti-TNF-α (1:200), anti-IL 6 (1:200), anti-MPO (1:200), anti-PECAM (1:200), or anti-VEGF (1:200) at 4 °C overnight. After washing three times, the sections were incubated with HRP-conjugated secondary antibodies at 37 °C for another 1 h. Dimethylaminoazobenzene (DAB) was then added to manifest positive areas. The H&E and IHC samples were examined using an orthographic microscope (Olympus Corp., Tokyo, Japan). In addition, immunofluorescence staining was also performed to detect the infiltration of lymphocytes in psoriatic skin. Anti-CD4 (1:200) and anti-CD8 (1:200) were used to identify $CD4^+$ or $CD8^+$ cells, respectively. Alexa Fluor® 647-conjugated second antibodies were used for localization. Fluorescence images were recorded using a fluorescent microscope (Olympus Corp., Tokyo, Japan). Quantification was performed using Image J.

2.10. *Determination of SOD activity and levels of MDA, IL-17 and IL-22*

The serum was achieved after centrifuging blood samples at 5,000 rpm for 15 min. The protein concentration was determined using the BCA kit. The MDA level and SOD activity were detected using the MDA assay kit and SOD assay kit according to the instructions from the manufacturer. For

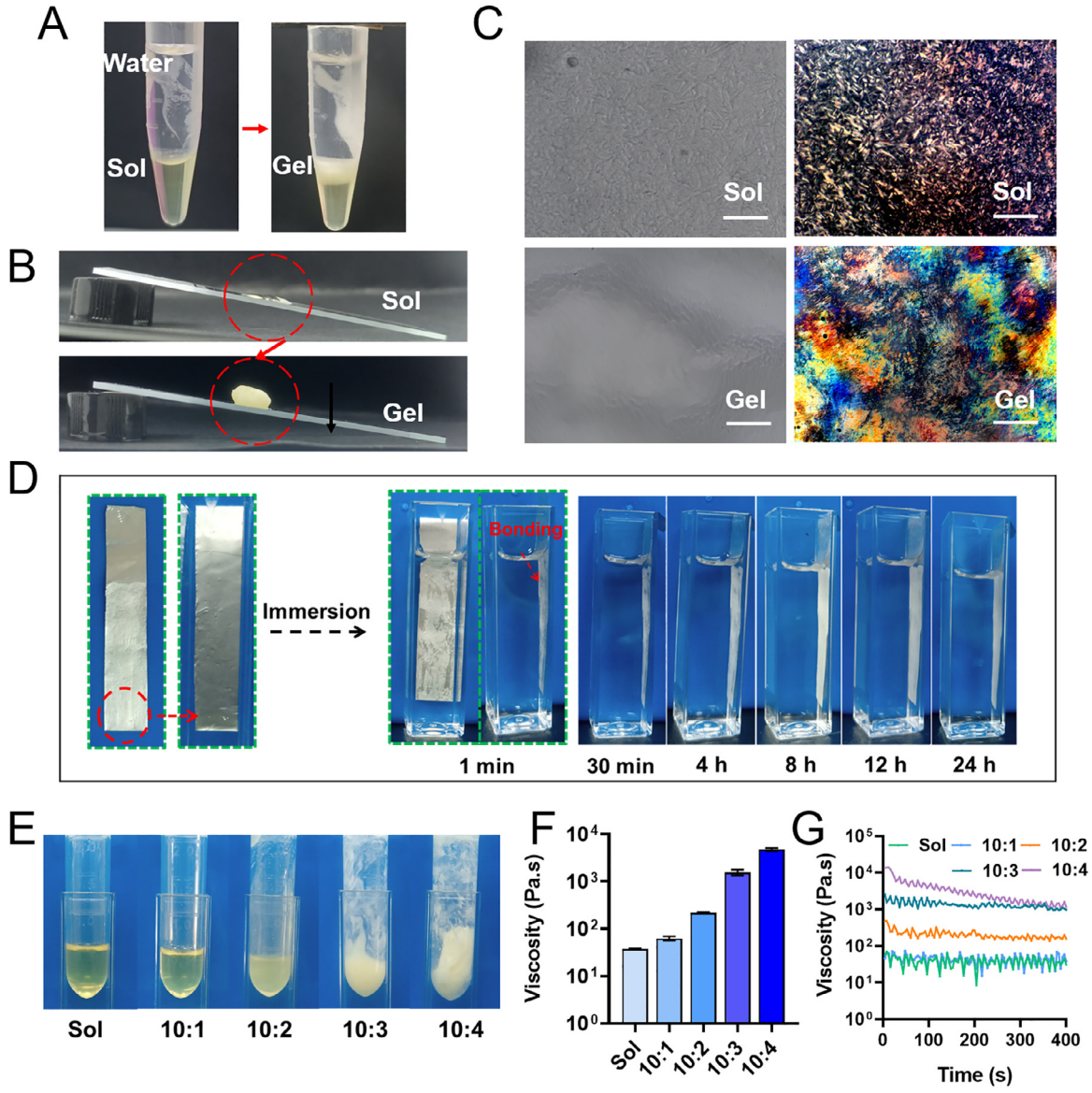

Fig. 1 – The water-triggered sol-gel phase transition property of WRG. (A) WRG turns from Sol state to Gel state after adding water in the tube. (B) Optical images of the Sol or Gel state of WRG on the slanted slide. (C) Inverted optical microscopy and polarized light microscopy (PLM) was used to visualize the Sol- or Gel state. Scale bar = 50 μM. (D) The WRG-Sol smeared tin foil could tightly adhere to the tube wall and last up to 24 h, indicating the strong adhesion property of WRG-Sol converting to WRG-Gel in the presence of water. (E) The appearance photographs. (F, G) The viscosity of WRG after mixing with different amounts of water. Data are presented as mean ± SEM in (F) and (H) (n = 3).

skin tissue, the samples were lysed by the lysis buffer and then centrifuged at 12,000 rpm for 10 min at 4 °C to collect the supernatant. The following procedure was the same as described above. IL-17 and IL-22 levels were determined using ELISA kits according to the manufacturer's instructions.

2.11. *Statistical analysis*

All statistical analysis was performed using GraphPad Prism 8.0 (Version 8.0, GraphPad Software, Inc., USA). All quantitative data were expressed as the mean ± standard error of mean (SEM). The differences among groups were assessed using Student's t-test or one-way analysis of variance with Tukey's post hoc test. $P < 0.05$ was considered to be significant.

3. Results and discussion

The water-responsive gel (WRG) was prepared using phosphatidyl choline (PC) and glyceryl dioleate (GDO), as described in the method section. To investigate the water-responsive gelation ability of WRG, we just added double distilled water into the tube containing WRG-Sol. As indicated in Fig. 1A, the transparently yellow converted

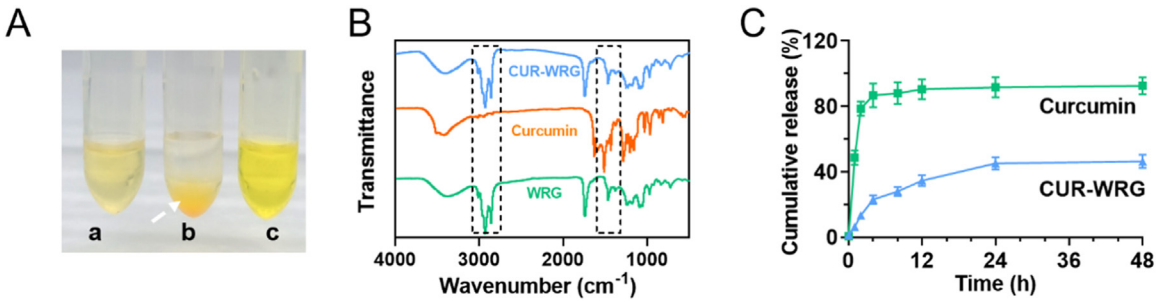

Fig. 2 – Characterization of curcumin loaded WRG formulation (CUR-WRG). (A) The photographs of a) CUR in DMSO, b) CUR in water, and c) CUR-WRG (Sol state). The white arrow indicates the undissolved CUR. (B) FTIR spectra of CUR, WRG, and CUR-WRG. (C) Cumulative release of CUR from free CUR or CUR-WRG in PBS (pH 7.4) containing 1% Tween 80. Data are presented as mean ± SEM (n = 3).

to milky white on the interface areas between the water phase and WRG-Sol phase, indicating the Sol-Gel phase transition. In the absence of water, the WRG-Sol was kept in a liquid state, evidenced by the photographs in Fig. 1B & S1. After mixing with water, the Sol-state was changed to Gel-state, and notably, the formed WRG-Gel could be sticking to the tube bottom or adhering to the slanted slide. As shown in Video S1, several drops of WRG-Sol were evenly spread on the glass slide; after spraying some water, the Sol WRG was quickly shifted to a Gel state, demonstrating the water triggered Sol-Gel phase transition property and the convenience of WRG for topical application. The Sol-Gel transition of WRG in the absence/presence of water was further visualized under a microscope (Fig. 1C). WRG-Sol showed a homogeneous dispersion; WRG-Gel was a bit humpy and hillocky but not very clear. Polarized light microscopy was further employed to investigate the dispersion state of WRG (Fig. 1C). The isotropous distribution of WRG-Sol was observed, whereas WRG-Gel showed significantly different morphology, indicating the Sol-Gel transition occurred. The above results demonstrated that WRG-Sol could quickly change to a Gel state after contacting with water. Interestingly, we found that the WRG-Gel could convert back to Sol state after losing water by keeping it at 37 °C for three days (Fig. S2). The phase transition could be two-way regulated by the water that exists in the formulation. In addition, we tested the adhesive property of WRG using a modified adhesion experiment based on the previously reported method [28]. As shown in Fig. 1D, a tin foil was smeared with WRG-Sol on one side and immersed in the water in a square-shaped tube. The phase transition of WRG happened within 1 min. The tin foil could tightly adhere to the tube wall and last up to 24 h, indicating the strong adhesion property of WRG-Gel. Therefore, WRG offers an interesting gel formulation with water triggered phase transition property, suitable for topical application.

We have demonstrated the water-triggered phase transition property of WRG. It is also of importance to investigate the water-responsiveness of WRG is applicable in practice. So, there is a question begs asking: How much water is sufficient to initiate the Sol-to-Gel transition? In the following experiments, we investigated the gelation process of WRG after adding different amounts of water to the WRG-Sol. As shown in Fig. 1E, the appearance of WRG was gradually changed from transparently yellow to milky white as the amount of water added increased. We further tested the viscosity (Fig. 1F & 1G) of WRG-Gel. The 10:1 (Sol: water, v/v) mixture achieved similar viscosity as WRG-Sol, indicating the 10: 1 mixture was maintained in the liquid state. The photograph in Fig. 1E showed 10: 1 mixture still presents a transparent color, consistent with the viscosity results. The increased water ratio in mixture further increased the viscosity, indicating the formation of WRG-Gel. In addition, the higher water ratio in mixture resulted in a stronger viscosity. The sol-gel transition of an aqueous solution usually accompanies changes in the hydration and the solute-binding of dispersed molecules [29,30]. Thus, the increased water ratio changed the hydration and water-binding condition of dispersed components in WRG, which might further affect the intra- and inter-molecular hydrogen bonding and initiate the phase transition. These data confirmed the water-triggered phase transition of WRG, and more importantly, a relatively small amount of water could initiate the gelation process, which provides more convenience for the use of WRG in practice. The water-responsive property of WRG make it more convenient for topical application by smearing. In addition, the involved additional water could also aid to keep the skin moistened, beneficial for drug delivery and psoriasis treatment.

To explore the biomedical use of WRG as a drug delivery carrier against psoriasis, CUR was selected as a model drug and loaded into WRG. As shown in Fig. 2A, CUR was easily dissolved in DMSO (a) but almost insoluble in the water, presenting as precipitates at the bottom of the tube (b). CUR could be completely dissolved in WRG-Sol, evidenced by the uniformed yellow color. This also demonstrates the strong drug loading capacity of WRG, which could be applied to most hydrophobic molecules. Additionally, FTIR was also carried out to investigate the involvement of CUR in the WRG system (Fig. 2B). WRG exhibited several characteristic absorption peaks, 2850 cm^{-1} and 2930 cm^{-1}, corresponding to C–H vibration. CUR showed 3400 cm^{-1} and 1520 cm^{-1}, corresponding to the O–H stretch band and C=O stretching vibrations. Most of the characteristic peaks in CUR were also presented in the spectrum of CUR-WRG, confirming the successful entrapment of CUR in WRG formulation. We

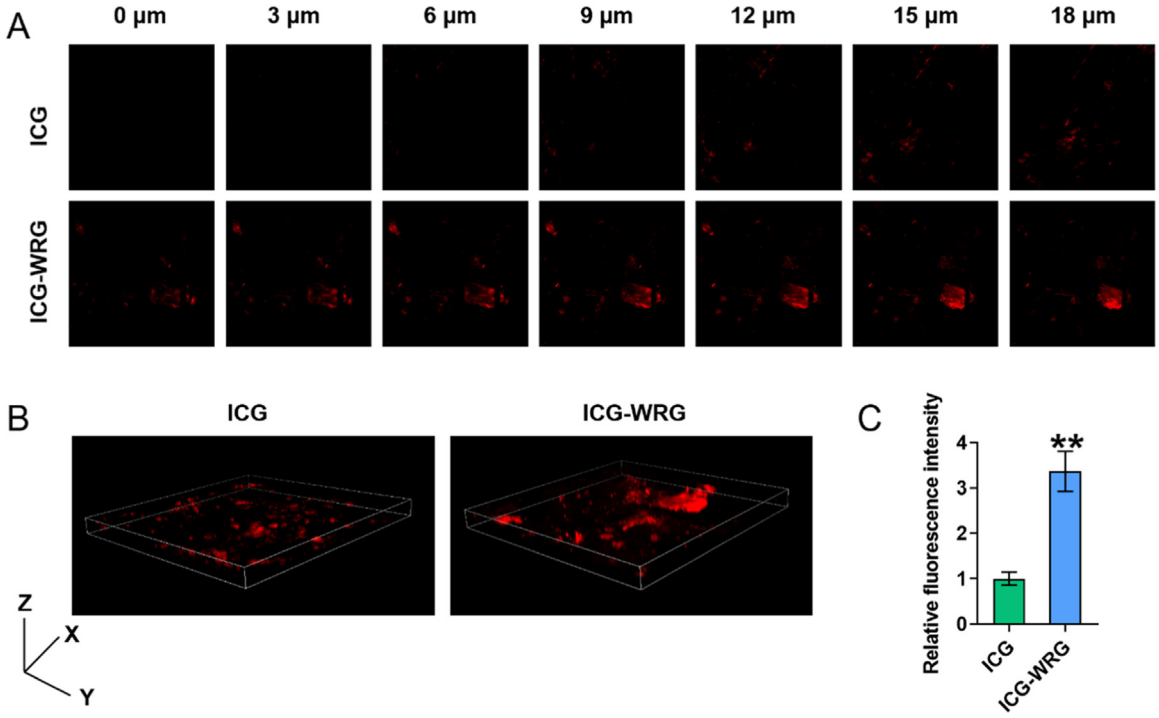

Fig. 3 – Enhanced permeation of ICG-WRG into psoriasis skin. (A) Representative confocal images of ear skin topically treated with ICG or ICG-WRG. Images were obtained at 3-μm intervals below the lateral ear skin surface. Scale bar = 100 μm. (B) Representative x-y-z orthogonal images of ICG- or ICG-WRG-treated ear skin. Vertical image length, 40 μm; Horizontal image length, 512 μm. (C) Relative fluorescence was quantified. Each value is represented as mean ± SEM ($n = 3$). **$P < 0.01$.

further investigate the *in vitro* release profile of CUR from WRG in PBS (pH 7.4) containing 1% Tween 80 (Fig. 2C). Free CUR was quickly released by over 80% in four hours, whereas CUR-WRG showed sustained release of CUR, and the cumulative release reached ~40% in 48 h. The significant difference should be attributed to the water-responsive gelation property of WRG. CUR-WRG could quickly shift to a gel state after being immersed in medium (Fig. 1) and keep the loaded drug for sustained release, while the free drug could be quickly released without any obstacle. These results suggested that CUR could be successfully loaded in WRG and sustainably released from the WRG. The enhanced solubility and sustained property of CUR in WRG make it suitable for topical application.

Drug retention and penetration are critical for topical drug delivery [31,32]. WRG could initiate Sol-Gel transition in the presence of water, and the formed gel with appropriate viscosity was beneficial for drug retention on the skin surface. To confirm this, we smeared the WRG-Sol on the back skin of the mouse and observed the *in-situ* gelation process after water spraying (Fig. S3). The WRG-Sol could be easily spread on the mouse skin due to the liquid state. An appropriate amount of water was spraying onto the mouse's back. Very quickly, the smeared WRG shifted to a gel state and tightly adhered to the mouse back skin (Fig. S3). These results demonstrated that water spraying could initiate the WRG gelation, and the formed gel could prolong skin retention compared to normal liquid preparations.

Following that, we further studied the drug molecules' penetration behavior in WRG. ICG was used as a fluorescence probe to track and visualize the penetration process when the WRG was topically administrated, and free ICG was utilized as the control. Three hours post topical administration and spraying water, the gel-state ICG-WRG was removed, and the ear tissue was cleaned for detection using a confocal microscope. Free ICG showed very weak fluorescence in all Z-stack images, while ICG-WRG showed a much stronger signal than free ICG (Fig. 3A). Furthermore, these data were reconstructed in 3D (Fig. 3B). It was observed that ICG-WRG showed stronger overall signals compared to free ICG, and the quantitative analysis was consistent (Fig. 3C). The WRG-mediated enhanced penetration enabled loaded drug traffic across the skin layer and reached the epidermis for functioning. These results suggested that WRG could not only improve the skin retention of loaded drugs but also facilitate the penetration of them into skin, which was suitable for topical drug delivery and psoriatic treatment. The enhanced penetration might be attributed to the extended retention, allowing drug permeation within a longer time. In addition, the components in WRG, like ethanol and PG could moisten the skin surface, aiding drug penetration [33,34]; PC, GDO, and Tween 80 could act as absorption enhancers and facilitate drug permeation to some exert [35–37]. The extended retention and the components in WRG synergistically contributed to the enhanced drug permeation into skin. It should be mentioned is that the psoriatic skin is intact compared to the heathy skin. The permeation

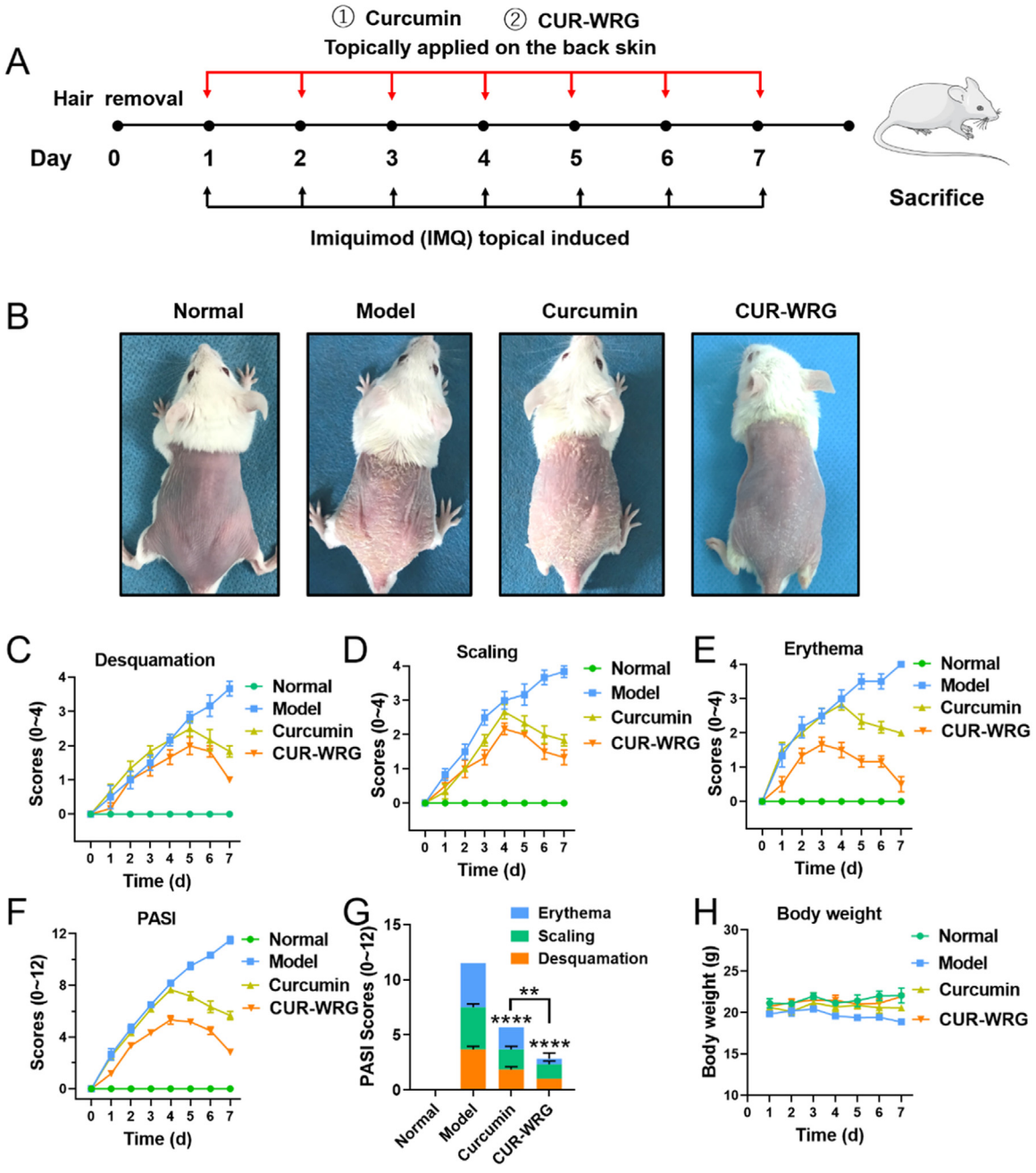

Fig. 4 – The therapeutic efficacy of CUR-WRG in a IMQ-induced psoriasis mouse model. (A) Representative gross images of mouse back skin after various treatments. The (B) erythema (C) desquamation (D) induration and (E) PASI scores of back skin lesions in psoriasis mice. (F) Total PASI scores of back skin lesions in psoriasis mice on Day 7. (G) The body weight was monitored and compared after varous treatments. Data are presented as mean ± SEM ($n = 6$). **$P < 0.01$, ****$P < 0.0001$.

behavior on the psoriatic and healthy skin of WRG-loaded drugs may be different. Admittedly, the psoriatic skin is more suitable for the evaluation of the preparations for psoriasis treatment. Comparatively, if WRG could facilitate drug penetration in healthy skin, it must be able to show enhanced drug permeation in psoriatic skin due to the intact skin barrier.

Preliminary results of animal experiments indicated that WRG formulation improves drug retention and penetration for topical use, which is inspiring. Before *in vivo* psoriasis treatment, we first studied the biocompatibility of WRG in HaCaT cells and healthy mice (Fig. S4). MTT assay was used to study the safety of WRG in HaCaT cells. As shown in Fig. S4A, negligible toxicity was observed in different concentrations of WRG. The WRG-Sol was further subcutaneously injected into the mouse's back. It is very interesting to observe the *in-situ* gelation of WRG occurs by absorbing the surrounding interstitial fluid. The appearance of WRG on Day 3 after subcutaneous injection was recorded (Fig. S4B). The skin tissue was collected after sacrificing the mouse, and the

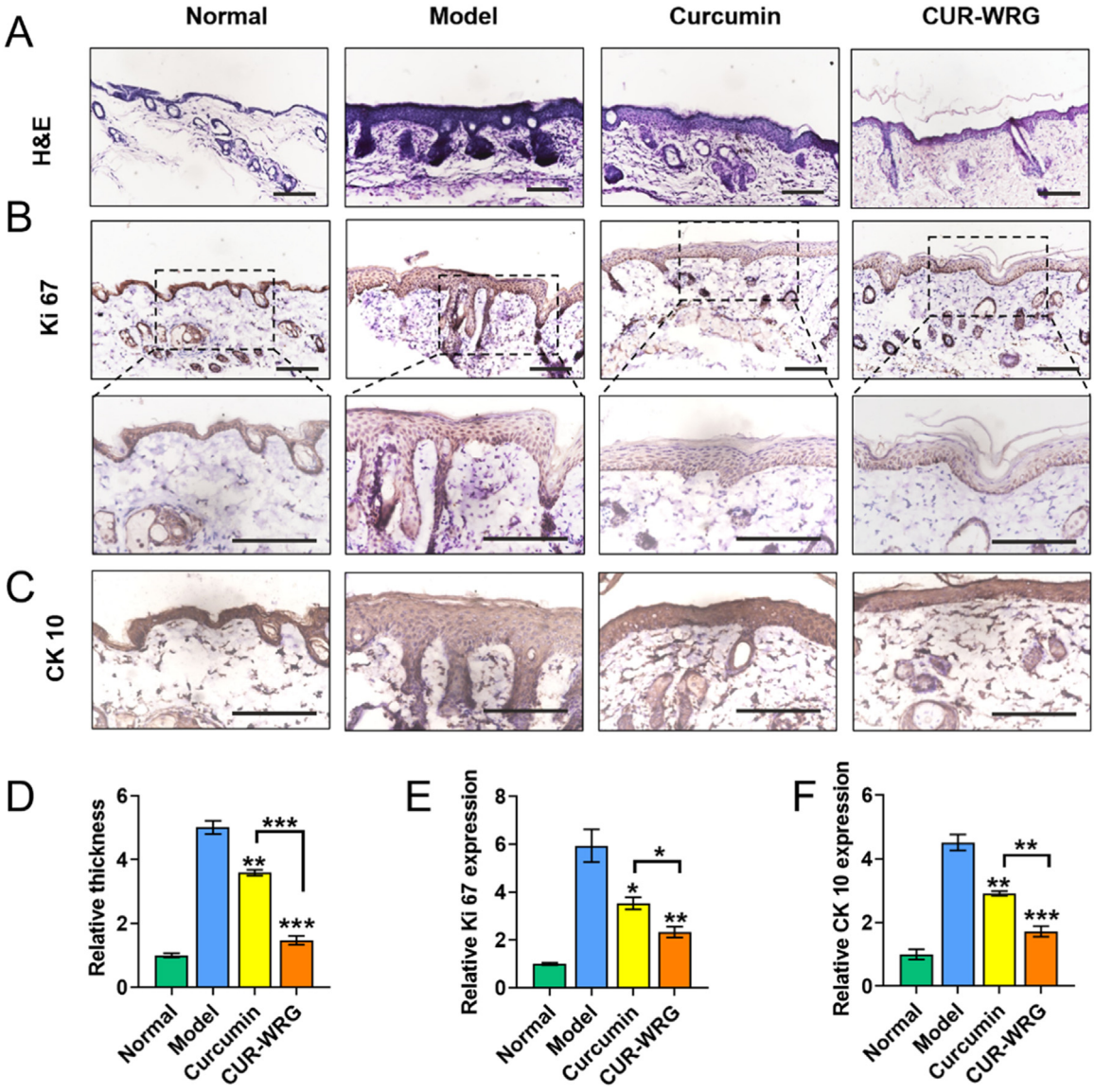

Fig. 5 – Histological analysis of the back skin of psoriasis mouse after various treatments. (A) H&E staining (scale bar = 100 μM). Immunohistochemical assay for (B) Ki 67 and (C) CK10 (scale bar = 100 μM). (D) Quantitative analysis for the relative epidermal thickenss. Quantitative analysis for the expression of (E) Ki 67 and (F) CK10. Data are presented as mean ± SEM ($n = 3$). *$P < 0.05$, **$P < 0.01$, ***$P < 0.001$.

appearance underneath the skin was also recorded (Fig. S4C). No abnormal swelling was observed in all groups. The collected skin tissue with subcutaneous injection of WRG showed similar features compared to the normal skin tissue (Fig. S5). Also, the skin tissue was sectioned for H&E staining. As shown in Fig. S4D, topical application and subcutaneous injection did not induce histological changes compared to the normal tissue. After 3 days following subcutaneous injection, the major organs were also collected, and H&E staining was performed for histological examination (Fig. S6). No changes were observed in the tested mice compared to the control mice. These results suggested that WRG holds acceptable biocompatibility for topical application and subcutaneous injection, allowing for further *in vivo* study.

We then tested the therapeutic effect of CUR-WRG against IMQ-induced ear psoriasis by topical administration. The whole experimental design graph is shown in Fig. 4A. After experiments, the mice were sacrificed, and the ear samples were collected, photographed, and sectioned for H&E staining (Fig. S7A). The ears in the IMQ-treated model group showed a thickening stratum corneum, while CUR-WRG treatment could significantly ameliorate IMQ-induced psoriatic stratum corneum. Free CUR also showed some therapeutic effects, but was significantly lower than CUR-WRG. The ear thickness (Fig. S7B) and relative keratin thickness (Fig. S7C) were also quantified, and both parameters were consistent with the ear phenotype. In addition, the PASI scores were also determined by monitoring the conditions of erythema, scaling, and desquamation in the psoriatic ear (Fig. S7D-S7G). The skin

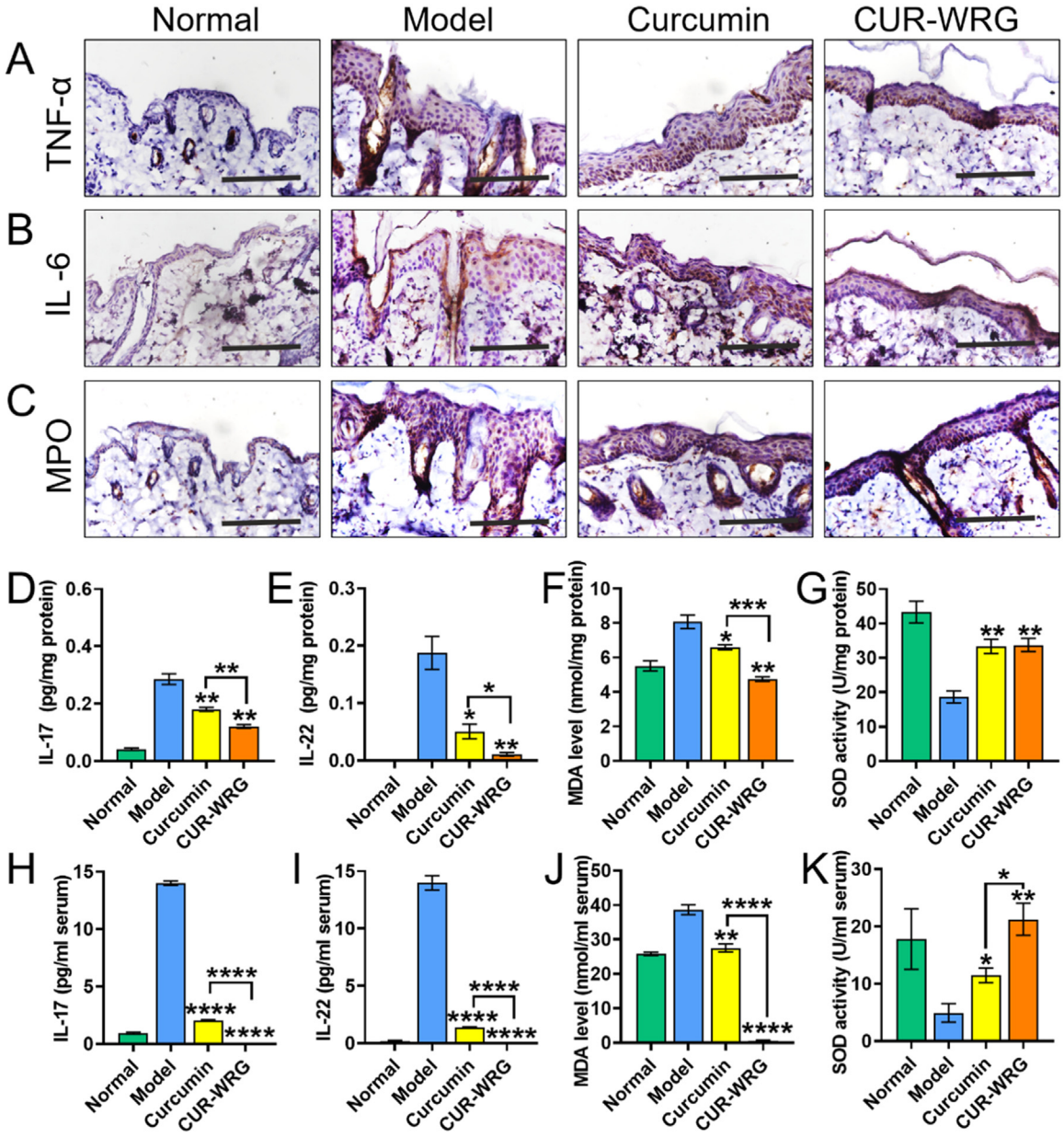

Fig. 6 – CUR-WRG treatment ameliorates psoriasis related inflammation and oxidative stress. Immunohistochemical assay for the expression of (A) TNF-α, (B) IL-6 and (C) MPO in the skin tissue (scale bar = 100 μM). ELISA assay for (D) IL-17 and (E) IL-22 levels in the skin tissue. (F) MDA and (G) SOD levels in the skin tissue. ELISA assay for (H) IL-17 and (I) IL-22 levels in the serum. (J) MDA levels and (K) SOD activities in the skin tissue. Data are presented as mean ± SEM ($n = 3$). *$P < 0.05$, **$P < 0.01$, ***$P < 0.001$, ****$P < 0.0001$.

erythema and desquamation in each group were increased for the first four consecutive days. Both CUR and CUR-WRG successfully reversed the upward trend, and CUR-WRG showed a stronger effect in attenuating these two symptoms. The scaling score in each group was increased in the first three days, and the trend was similar to that in erythema or desquamation. On the seventh day, the model group reached its highest PASI score (Fig. S7H). Free CUR decreased the PASI to some extent, which could be attributed to the anti-inflammation property of CUR itself. CUR-WRG further decreased the PASI score to ~1. The increased viscosity of WRG resulted in delayed drug retention (Fig. S3) and enhanced drug penetration (Fig. 3), thus helping to maximize the drug effect of CUR.

We also investigated the anti-psoriasis efficacy of CUR-WRG in an IMQ-induced psoriasis mouse model on the dorsal skin. The experimental design was similar, as shown in Fig. 4A, other than the psoriatic lesions were induced on the back skin. As shown in Fig. 4B, the model mice showed distinct scaly and thickened skin on the back. Both CUR and CUR-WRG exerted therapeutic efficacy to alleviate the skin symptoms. Compared to CUR, CUR-WRG gave a better performance with very less

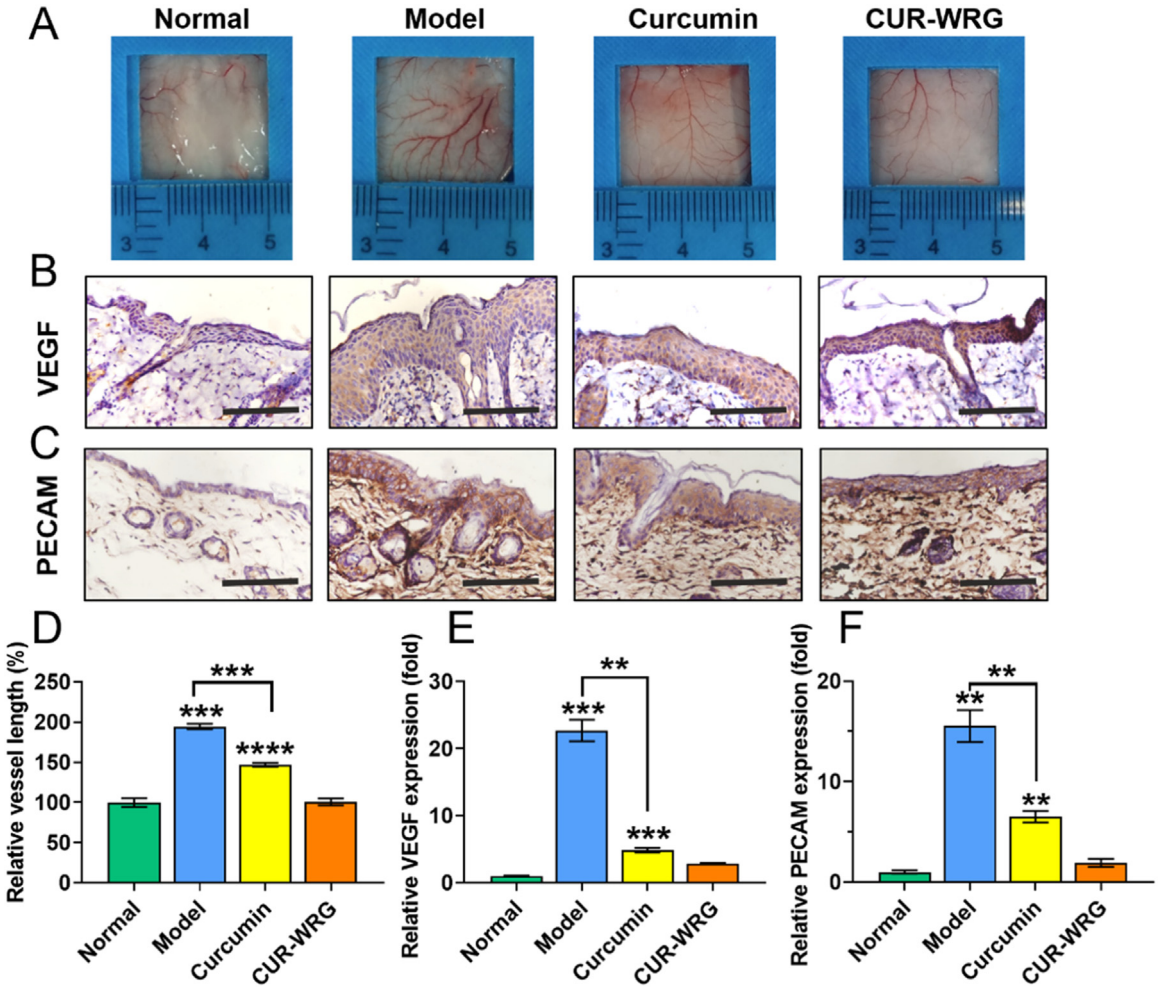

Fig. 7 – CUR-WRG treatment attenuates psoriasis induced epidermal angiogenesis. (A) The presentation of vessels in the back skin. Immonohistochemical assay for the expression of (B) VEGF and (C) PECAM in skin tissue (scale bar = 100 μM). (D) Quantitative analysis of relative vessel length. The quantification of the expression of (E) VEGF and (F) PECAM in skin tissue. Data are presented as mean ± SEM ($n = 3$). **$P < 0.01$, ***$P < 0.001$, ****$P < 0.0001$.

scaly skin left. The PASI scores based on skin desquamation, scaling, and erythema were also recorded and compared (Fig. 4C-4F). As the test proceeds, the model group showed an increased score in every aspect. Topical application of CUR or CUR-WRG started to decrease these scores on the third to fifth day (Fig. 4C-4F), which was consistent with the ear results (Fig. S5D-S5G). On the seventh day, the model group showed the highest PASI score, while both CUR and CUR-WRG treatment decreased the score, but not at the same level (Fig. 4G). CUR-WRG presented a better therapeutic efficacy, which could be attributed to the delayed drug retention by the increased viscosity (Fig. S3) and the facilitated drug penetration (Fig. 3). In addition, the body weight was also monitored (Fig. 4H). IMQ exposure resulted in significant weight loss in the model group [38] . The weight-loss effect in the CUR treatment group was lower, indirectly reflecting the relieved psoriasis progression. The mice in the CUR-WRG group had similar body weight as the normal group, demonstrating the superior therapeutic efficacy and the biological safety of CUR-WRG against psoriasis.

After the experiments, the skin samples were collected for histological analysis. As shown in Fig. 5A, the basal and upper basal hyperplasia, vascular hyperplasia, and infiltration of inflammatory cells were observed in the H&E staining in the model group. This data was consistent with previously reported data [25,38], and confirmed the successful development of the psoriasis mouse model. CUR treatment alleviated these histological characteristics in the skin tissue with IMQ exposure. CUR-WRG showed the most potent therapeutic effect against IMQ-induced psoriasis, evidenced by the decreased basal hyperplasia, vascular hyperplasia, and infiltration of inflammatory cells in psoriatic skin, and the treated back skin recovered back to that similar to healthy skin. The relative skin thickness also confirmed these results (Fig. 5D). Keratinocyte hyperproliferation is one of the crucial pathological changes in psoriatic skin. Therefore, we further analyzed the expression of Ki 67, a biomarker for proliferation, in skin samples using an immunohistochemical assay (Fig. 5B & 5E). The expression of Ki67 was increased along with the thickened basal of the epidermis. The increased Ki67

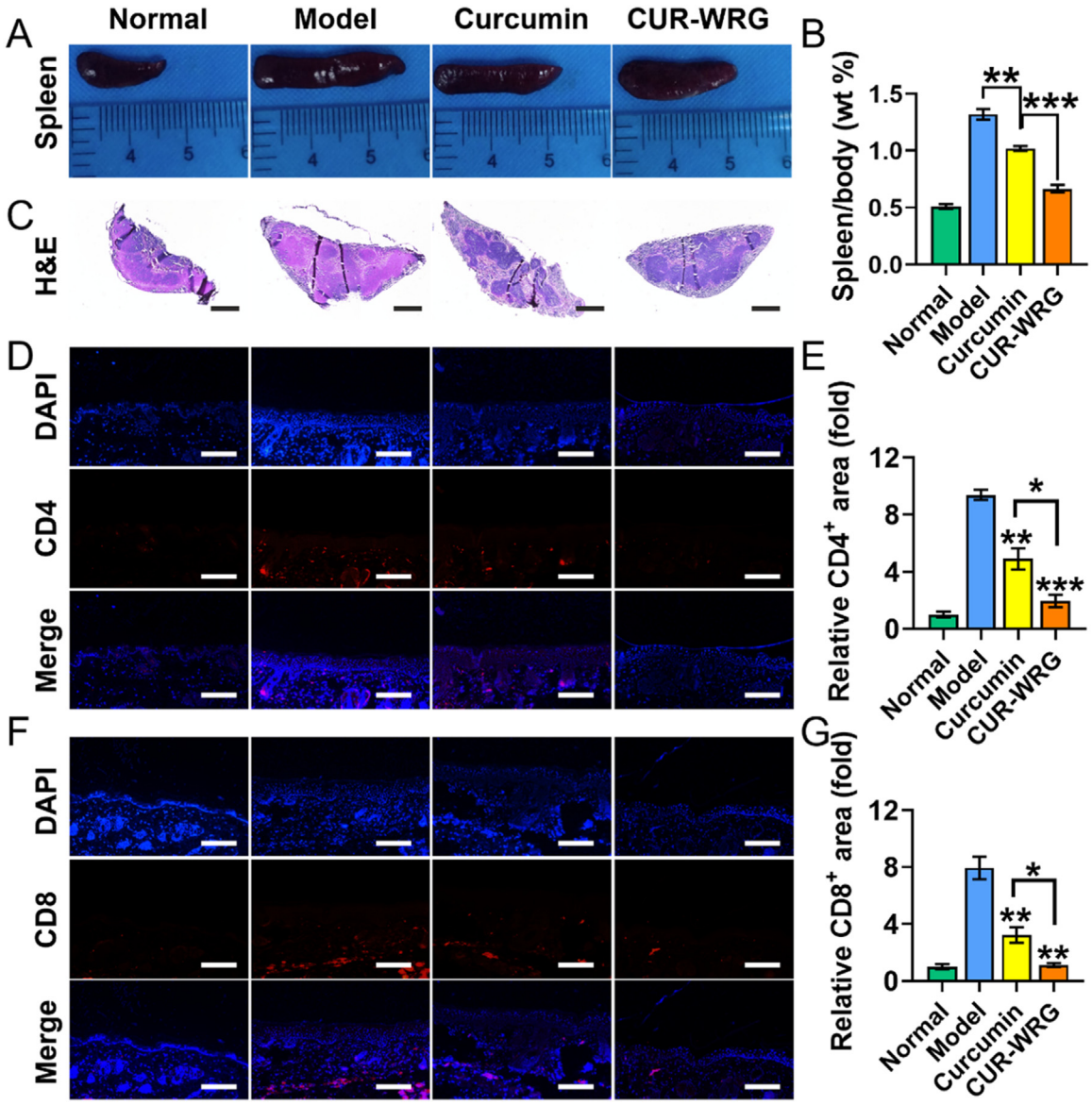

Fig. 8 – CUR-WRG treatment suppresses psoriasis induced splenomegaly and restricts T lymph cells recruitment. (A) The photograph of spleen on Day 7. (B) the spleen/body weight ratio. (C) H&E staining of the spleen. The immunofluorescence staining of (D) CD4 and (F) CD8 in skin tissue. Quantitative analysis of (E) CD4 and (G) CD8. Scale bar = 100 μM. *P < 0.05, **P < 0.01, ***P < 0.001.

expression reflected the hyperplasia of skin tissue after IMQ exposure. CUR and CUR-WRG both decreased the Ki 67 expression, while CUR-WRG exhibited a stronger suppressing effect. Cytokeratin 10 (CK10) was also used to indicate the proliferation state of keratinocytes (Fig. 5C & 5F). IMQ exposure significantly improved the expression of CK 10, while CUR and CUR-WRG largely offset this increase. Quantitative analysis of CK10 (Fig. 5F) showed a similar trend as the Ki67 expression (Fig. 5E). Collectively, these data suggested that CUR-WRG could suppress the hyperproliferation in psoriatic skin by decreasing Ki67 and CK10 expression in a psoriasis model.

Psoriasis is associated with mild chronic inflammation that increases oxidative stress and causes cell and tissue damage. So, we further detected the impact of CUR-WRG on skin inflammation and oxidative stress in psoriasis mice. TNF-α and IL-6 have been widely reported to be involved in the development of psoriasis and are also regarded as indications for disease severity [39–41]. The corresponding inhibitors or antagonists have been explored to treat psoriasis and showed considerable efficacy [42,43]. In our results, IMQ exposure significantly increased the expression of TNF-α (Fig. 6A and S8A) and IL-6 (Fig. 6B and S8B) in skin tissue. Both CUR and CUR-WRG showed a considerable effective suppressing effect, evidenced by the downregulation of TNF-α and IL-6 after treatments. Of course, CUR-WRG possessed a stronger effect. These results were consistent with the better appearance of mice in the CUR-WRG group (Fig. 4).

Clinical data demonstrated that Th17 cells are highly involved in the pathogenesis of psoriasis [44]. Th17 could release inflammatory cytokines (including IL-17 and

IL-22), which induced a series of changes, like keratinocyte hyperproliferation, dermal blood vessel hyperplasia, and leukocyte infiltration into the dermis etc., exacerbating the psoriatic condition [44]. Therefore, we further monitored the IL-17 and IL-22 levels in both skin and serum to evaluate the Th17 activation and psoriatic condition by ELISA assay. As shown in Fig. 6D & 6E, the IMQ-induced model group showed a significantly increased amount of IL-17 and IL-22 in skin tissues. It should be mentioned that the serum amount of IL-17 and IL-22 of mice in the model group was drastically increased (Fig. 6H & 6I). These data suggested that IMQ exposure aggressively activated Th17 and boosted the release of IL-17 and IL-22. As expected, CUR and CUR-WRG decreased the inflammatory cytokine in both skin tissue and serum, and CUR-WRG robustly decreased the IL-17 and IL-22 levels, exerting a much stronger effect than CUR.

The increased oxidative stress also plays a key role in the psoriasis development, and the psoriatic skin often remains hyperoxidized [45]. Thus, we examined the expression of MPO, a bridge linking inflammation and oxidative stress, by immunohistochemical assay. As shown in Fig. 6C and S8C, IMQ exposure significantly elevated the MPO expression, which could be contracted by CUR and CUR-WRG, and CUR-WRG exerted a much stronger effect than CUR due to the enhanced retention and penetration. Furthermore, we also studied the MDA level and SOD activity in skin tissue and serum to indicate the redox state after various treatments. MDA in skin tissue was elevated by IMQ exposure but decreased after CUR-involved treatment (Fig. 6F). Similarly, the increased serum MDA level was also suppressed by CUR or CUR-WRG treatment (Fig. 6J). More surprisingly, CUR-WRG decreased the serum MDA level to a lower level as compared to that of healthy mice. Therefore, CUR-WRG could effectively suppress IMQ-induced hyperoxidation in both skin tissue and serum. Conversely, SOD activity was decreased in the model group in both skin tissue and serum but elevated by CUR formulations (Fig. 6G & 6K). Taken together, it was suggested that IMQ exposure could induce hyperoxidition and oxidative stress, but the redox state could be effectively corrected back to a normal level with CUR-WRG topical treatment.

Angiogenesis is also one of the obvious characteristics of psoriasis, and vascular proliferations and abnormalities of dermal blood vessels often occur during different stages of psoriasis [46–48]. Several anti-angiogenesis agents have been reported to treat psoriasis by topical administration or systemic application [49,50]. Here, we also detected the vascular alterations to further understand the therapeutic effect of CUR-WRG (Fig. 7). In the model group, IMQ exposure induced significant blood vessel dilation and new branched vessel formation (Fig. 7A). Both CUR and CUR-WRG showed an inhibitory effect on neovascularization in the psoriatic lesions. Quantitative analysis demonstrated that CUR-WRG decreased the vessel length and density to normal, demonstrating its potential therapeutic efficacy (Fig. 7D and S9). We further studied the expression of VEGF and PECAM, two classic biomarkers for neovascularization, with an immunohistochemical assay (Fig. 7B & 7C). Strong signals that represent VEGF or PECAM were observed in the model group, suggesting the high activity of vascularization. CUR and CUR-WRG treatment significantly decreased the expression of these two biomarkers, and the quantitative analysis (Fig. 7E & 7F) was consistent. So CUR could inhibit angiogenesis by decreasing VEGF and PECAM expression, which contribute to the anti-psorisis therapy, and meanwhile, WRG formulation amplified the therpeutic effect of CUR against psoriasis.

Spleen is usually enlarged in psoriatic patients due to the overreacted immune system. Spleen harbors many immune cells and plays a critical role in immune function. Here, we also monitored the spleen condition after various treatments. As shown in Fig. 8A, the spleen in the model group had a bigger size compared to that in the normal group, and the spleen/body ratio was significantly increased (about 3-fold), indicating the increased immune cell number and activated immunization in the psoriatic spleen (Fig. 8B). CUR and CUR-WRG treatments decreased the spleen size as well as the spleen/body ratio, indicating a considerable immunomodulation function. As expected, CUR-WRG presented a stronger effect on this aspect compared to free CUR. The spleen tissue was further sectioned for H&E staining. As shown in Fig. 8C, the white pulp, comprising lymph-related nodules rich in T cells and macrophages, was significantly expanded in the model group compared to that in the normal group. CUR-WRG treatment dramatically decreased the number of lymph-related nodules, which is more significant than CUR treatment. So, CUR-WRG could suppress psoriasis associated systemic immune activation. Then, we further determined the infiltration of T cells in psoriatic lesions. As shown in Fig. 8D-8G, we examined the presentation of CD4+ and CD8+ cells in psoriatic skin after various treatments. Plenty of CD4+ and CD8+ cells were recruited to the psoriatic skin after IMQ exposure, and the increase was up to about 9 folds and 8 folds. We noticed that CUR could reduce the infiltration of T CD4+ and CD8+ cells while using WRG as a delivery carrier could further enhance its drug action. The suppressed systemic immune activation (Fig. 8A-8C) could also contribute to the decreased infiltration of T lymphocytes in skin. Taken together, CUR-WRG could modulate systemic immune activation and decrease T lymphocyte infiltration in psoriatic skin lesions.

4. Conclusion

In this study, we developed a gel formulation, WRG, with water-triggered sol-gel phase transition property and validated its potential as a CUR topical deliver carrier for psoriasis treatment. CUR-WRG prolonged the skin retention of CUR and enhanced the drug permeation into psoriatic skin tissue in a psoriasis mouse model. *In vivo* data confirmed that CUR-WRG could ampliefied the anti-hyperplasia, anti-inflammation, anti-angiogenesis, anti-oxidation, and immunomodulation properties of CUR, effectively amerliorating the psoriasis symtoms and exerting robust anti-psoriatic effect. Notably, the CUR-WRG showed neglectable local and systemic toxicity, evidenced by the histological analysis in healthy mice and stable body weight in psoriatic mice. In summary, WRG provided a promising drug delivery carrier for topically psoriatic treatment.

Conflicts of interest

The authors declare no conflict of interest.

Acknowledgements

This research was supported by National Natural Science Foundation of China (Grant No. 81903551), Natural Science Foundation of Zhejiang Province (Grant No. LYY22H300001), Wenzhou Municipal Science and Technology Bureau (Grant No. ZY2019007), Zhejiang postdoctoral scientific research project (Grant No. ZJ2021024), Wenzhou Municipal Key Laboratory of Pediatric Pharmacy (Grant No. WZEY02) and Excellent Young Scientist Training Program fund from Wenzhou Medical University.

Supplementary materials

Supplementary material associated with this article can be found, in the online version, at doi:10.1016/j.ajps.2023.100782.

References

[1] Grozdev I, Korman N, Tsankov N. Psoriasis as a systemic disease. Clin Dermatol 2014;32(3):343–50.
[2] Lebwohl M. Psoriasis. Ann Intern Med 2018;168(7):Itc49–64.
[3] Hawkes JE, Chan TC, Krueger JG. Psoriasis pathogenesis and the development of novel targeted immune therapies. J Allergy Clin Immunol 2017;140(3):645–53.
[4] Rudnicka L, Olszewska M, Goldust M, Waskiel-Burnat A, Warszawik-Hendzel O, Dorozynski P, et al. Efficacy and safety of different formulations of calcipotriol/betamethasone dipropionate in psoriasis: gel, foam, and ointment. J Clin Med 2021;10(23):5589.
[5] Tachibana K, Tang N, Urakami H, Kajita A, Kobashi M, Nomura H, et al. Multifaceted analysis of IL-23A- and/or EBI3-including cytokines produced by psoriatic keratinocytes. Int J Mol Sci 2021;22(23):12659.
[6] Greb JE, Goldminz AM, Elder JT, Lebwohl MG, Gladman DD, Wu JJ, et al. Psoriasis. Nat Rev Dis Primers 2016;2:16082.
[7] Wang H, Su D, Huang R, Shu F, Cheng F, Zheng G. Cellular nanovesicles with bioorthogonal targeting enhance photodynamic/photothermal therapy in psoriasis. Acta Biomater 2021;134:674–85.
[8] Furuhashi T, Saito C, Torii K, Nishida E, Yamazaki S, Morita A. Photo(chemo)therapy reduces circulating Th17 cells and restores circulating regulatory T cells in psoriasis. PLoS One 2013;8(1):e54895.
[9] Zheng J, Chen W, Gao Y, Chen F, Yu N, Ding Y, et al. Clinical analysis of generalized pustular psoriasis in Chinese patients: a retrospective study of 110 patients. J Dermatol 2021;48(9):1336–42.
[10] Wang J, Wang YM, Ahn HY. Biological products for the treatment of psoriasis: therapeutic targets, pharmacodynamics and disease-drug-drug interaction implications. AAPS J 2014;16(5):938–47.
[11] Castela E, Archier E, Devaux S, Gallini A, Aractingi S, Cribier B, et al. Topical corticosteroids in plaque psoriasis: a systematic review of efficacy and treatment modalities. J Eur Acad Dermatol Venereol 2012;26(Suppl 3):36–46.
[12] Takahashi H, Katayama H, Uwajima Y, Koda M, Sasaki H, Tanito K, et al. Patient satisfaction and efficacy of calcipotriol plus betamethasone dipropionate gel in plaque psoriasis patients with poor adherence. J Dermatol 2020;47(11):1249–56.
[13] Bewley A, Page B. Maximizing patient adherence for optimal outcomes in psoriasis. J Eur Acad Dermatol Venereol 2011;25(Suppl 4):9–14.
[14] Huang YB, Lin YH, Lu TM, Wang RJ, Tsai YH, Wu PC. Transdermal delivery of capsaicin derivative-sodium nonivamide acetate using microemulsions as vehicles. Int J Pharm 2008;349(1–2):206–11.
[15] Sun L, Liu Z, Wang L, Cun D, Tong HHY, Yan R, et al. Enhanced topical penetration, system exposure and anti-psoriasis activity of two particle-sized, curcumin-loaded PLGA nanoparticles in hydrogel. J Controll Rel 2017;254:44–54.
[16] Hadizadeh M, Naeimi M, Rafienia M, Karkhaneh A. A bifunctional electrospun nanocomposite wound dressing containing surfactin and curcumin: *in vitro* and *in vivo* studies. Mater Sci Eng C 2021;129:112362.
[17] Chen Y, Jiang Z, Xu J, Zhang J, Sun R, Zhou J, et al. Improving the ameliorative effects of berberine and curcumin combination via dextran-coated bilosomes on non-alcohol fatty liver disease in mice. J Nanobiotechnol 2021;19(1):230.
[18] Yuyun Y, Ratnatilaka Na Bhuket P, Supasena W, Suwattananuruk P, Praengam K, Vajragupta O, et al. A novel curcumin-mycophenolic acid conjugate inhibited hyperproliferation of tumor necrosis factor-alpha-induced human keratinocyte cells. Pharmaceutics 2021;13(7):956.
[19] Nosrati H, Attari E, Abhari F, Barsbay M, Ghaffarlou M, Mousazadeh N, et al. Complete ablation of tumors using synchronous chemoradiation with bimetallic theranostic nanoparticles. Bioact Mater 2022;7:74–84.
[20] Cao S, Wang C, Yan J, Li X, Wen J, Hu C. Curcumin ameliorates oxidative stress-induced intestinal barrier injury and mitochondrial damage by promoting Parkin dependent mitophagy through AMPK-TFEB signal pathway. Free Radic Biol Med 2020;147:8–22.
[21] Li H, Liu T, Zhu Y, Fu Q, Wu W, Deng J, et al. An in situ-forming phospholipid-based phase transition gel prolongs the duration of local anesthesia for ropivacaine with minimal toxicity. Acta Biomater 2017;58:136–45.
[22] Kou L, Sun R, Jiang X, Lin X, Huang H, Bao S, et al. Tumor microenvironment-responsive, multistaged liposome induces apoptosis and ferroptosis by amplifying oxidative stress for enhanced cancer therapy. ACS Appl Mater Interfaces 2020;12(27):30031–43.
[23] Kou L, Jiang X, Tang Y, Xia X, Li Y, Cai A, et al. Resetting amino acid metabolism of cancer cells by $ATB^{0,+}$-targeted nanoparticles for enhanced anticancer therapy. Bioactive materials 2022;9:15–28.
[24] Fonseca-Santos B, Gremião MPD, Chorilli M. A simple reversed phase high-performance liquid chromatography (HPLC) method for determination of *in situ* gelling curcumin-loaded liquid crystals in *in vitro* performance tests. Arabian J Chem 2017;10(7):1029–37.
[25] Chen R, Zhai YY, Sun L, Wang Z, Xia X, Yao Q, et al. Alantolactone-loaded chitosan/hyaluronic acid nanoparticles suppress psoriasis by deactivating STAT3 pathway and restricting immune cell recruitment. Asian J Pharm Sci 2022;17(2):268–83.
[26] Catlett IM, Hu Y, Gao L, Banerjee S, Gordon K, Krueger JG. Molecular and clinical effects of selective tyrosine kinase 2 inhibition with deucravacitinib in psoriasis. J Allergy Clin Immunol 2022;149(6) 2010–20.e8.
[27] Yao Q, Jiang X, Zhai YY, Luo LZ, Xu HL, Xiao J, et al. Protective effects and mechanisms of bilirubin nanomedicine against acute pancreatitis. J Controll Rel 2020;322:312–25.
[28] Yu D, Huang J, Zhang Z, Weng J, Xu X, Zhang G, et al. Simultaneous realization of superoleophobicity and strong

substrate adhesion in water via a unique segment orientation mechanism. Adv Mater 2022;34(2):e2106908.
[29] Miyawaki O, Omote C, Matsuhira K. Thermodynamic analysis of sol-gel transition of gelatin in terms of water activity in various solutions. Biopolymers 2015;103(12):685–91.
[30] Miyawaki O, Norimatsu Y, Kumagai H, Irimoto Y, Kumagai H, Sakurai H. Effect of water potential on sol-gel transition and intermolecular interaction of gelatin near the transition temperature. Biopolymers 2003;70(4):482–91.
[31] Svendsen MT, Feldman SR, Moller S, Kongstad LP, Andersen KE. Long-term improvement of psoriasis patients' adherence to topical drugs: testing a patient-supporting intervention delivered by healthcare professionals. Trials 2021;22(1):742.
[32] Svendsen MT, Feldmann S, Tiedemann SN, Sorensen ASS, Rivas CMR, Andersen KE. Improving psoriasis patients' adherence to topical drugs: a systematic review. J Dermatolog Treat 2020;31(8):776–85.
[33] Zhang Y, Xia Q, Li Y, He Z, Li Z, Guo T, et al. CD44 assists the topical anti-psoriatic efficacy of curcumin-loaded hyaluronan-modified ethosomes: a new strategy for clustering drug in inflammatory skin. Theranostics 2019;9(1):48–64.
[34] Carrer V, Alonso C, Pont M, Zanuy M, Córdoba M, Espinosa S, et al. Effect of propylene glycol on the skin penetration of drugs. Arch Dermatol Res 2020;312(5):337–52.
[35] Kim C, Shim J, Han S, Chang I. The skin-permeation-enhancing effect of phosphatidylcholine: caffeine as a model active ingredient. J Cosmet Sci 2002;53(6):363–74.
[36] Dante MCL, Borgheti-Cardoso LN, Fantini MCA, Praça FSG, Medina WSG, Pierre MBR, et al. liquid crystalline systems based on glyceryl monooleate and penetration enhancers for skin delivery of celecoxib: characterization, *in vitro* drug release, and *in vivo* studies. J Pharm Sci 2018;107(3):870–8.
[37] Zhang H, Yao M, Morrison RA, Chong S. Commonly used surfactant, Tween 80, improves absorption of P-glycoprotein substrate, digoxin, in rats. Arch Pharm Res 2003;26(9):768–72.
[38] Jiang X, Yao Q, Xia X, Tang Y, Sun M, Li Y, et al. Self-assembled nanoparticles with bilirubin/JPH203 alleviate imiquimod-induced psoriasis by reducing oxidative stress and suppressing Th17 expansion. Chem Eng J 2022;431:133956.
[39] Lin L, Wang Y, Lu X, Wang T, Li Q, Wang R, et al. The inflammatory factor SNP may serve as a promising biomarker for acitretin to alleviate secondary failure of response to TNF-a monoclonal antibodies in psoriasis. Front Pharmacol 2022;13:937490.
[40] Saggini A, Chimenti S, Chiricozzi A. IL-6 as a druggable target in psoriasis: focus on pustular variants. J Immunol Res 2014;2014:964069.
[41] Hunter CA, Jones SA. IL-6 as a keystone cytokine in health and disease. Nat Immunol 2015;16(5):448–57.
[42] Sola-Ortigosa J, Sánchez-Regaña M, Umbert-Millet P. Efficacy of adalimumab in the treatment of psoriasis: a retrospective study of 15 patients in daily practice. J Dermatolog Treat 2012;23(3):203–7.
[43] Ravipati A, Nolan S, Alphonse M, Dikeman D, Youn C, Wang Y, et al. IL-6R/signal transducer and activator of transcription 3 signaling in keratinocytes rather than in T cells induces psoriasis-like dermatitis in mice. J Invest Dermatol 2022;142(4) 1126–35.e4.
[44] Keijsers RR, Joosten I, van Erp PE, Koenen HJ, van de Kerkhof PC. Cellular sources of IL-17 in psoriasis: a paradigm shift? Exp Dermatol 2014;23(11):799–803.
[45] Zhou Q, Mrowietz U, Rostami-Yazdi M. Oxidative stress in the pathogenesis of psoriasis. Free Radic Biol Med 2009;47(7):891–905.
[46] Kelly AG, Panigrahy D. Targeting angiogenesis via resolution of inflammation. Cold Spring Harb Perspect Med 2022:a041172.
[47] Luengas-Martinez A, Paus R, Young HS. Antivascular endothelial growth factor-A therapy: a novel personalized treatment approach for psoriasis. Br J Dermatol 2022;186(5):782–91.
[48] Afonina IS, Van Nuffel E, Beyaert R. Immune responses and therapeutic options in psoriasis. Cell Mol Life Sci 2021;78(6):2709–27.
[49] Arbiser JL. Fumarate esters as angiogenesis inhibitors: key to action in psoriasis? J Invest Dermatol 2011;131(6):1189–91.
[50] Liu W, Zhang D, Luo M, Jia F, Peng L, Li X, et al. TNF-like weak inducer of apoptosis promotes angiogenesis, thereby exacerbating cutaneous psoriatic disease. J Invest Dermatol 2021;141(5) 1356–60 e8.